JOURNAL OF CATALYSIS 154, 98–106 (1995)

Structure and Chemical Composition of a Supported Pt–Ru Electrocatalyst for Methanol Oxidation

V. Radmilović,[1] H. A. Gasteiger, and P. N. Ross, Jr.

National Center for Electron Microscopy, and Materials Sciences Division, Lawrence Berkeley Laboratory, University of California, Berkeley, California 94720

Received September 29, 1994; revised February 16, 1995

High resolution electron microscopy and X-ray microchemical analysis were used to characterize the composition, size, distribution, and morphology of Pt–Ru particles with nominal Pt:Ru ratios of 1:1 and 3:1, supported on carbon black. The particles are predominantly single nanocrystals with diameters in the order of 2.0 to 2.5 nm. Occasionally, twinned particles are also observed. All investigated particles represent solid solutions of Pt and Ru with compositions very close to the nominal one. Based on two-dimensional projection in high resolution images, it is suggested that the well-resolved particles are of cubooctahedral shape. In addition to {200} and {111} facets, {113} facets are also observed. © 1995 Academic Press, Inc.

1. INTRODUCTION

Bimetallic alloy particles supported on high surface area carbon find widespread application as electrode materials. Of particular interest are platinum–ruthenium alloys used for the electrooxidation of methanol at the anode of low temperature fuel cells (e.g., 1–3). In heterogenous catalysis, supported platinum–ruthenium has been studied as a catalyst for methanation (4), alkane hydrogenolysis (5), and alkene hydrogenation (6). The choice of precursor molecules and formation conditions in the preparation of bimetallic Pt–Ru catalysts strongly affects the dispersion and the compositional homogeneity of the alloy clusters (7, 8), both of which are important factors in determining their electrocatalytic activity toward methanol oxidation (9). In previous work (9), we have shown that the catalytic activity of bulk Pt–Ru alloy is extremely sensitive to the surface composition, with the alloy having optimum surface composition (ca. 10 at.% Ru) being approximately two orders of magnitude more active than pure Pt and several orders of magnitude more active than pure Ru. Therefore, it is clearly of importance to verify the desired compositional homogeneity of the supported bimetallic particles, i.e., to assess the extent of alloy formation. Furthermore, as the utilization of the precious metals is inversely related to the particle size, their dispersion should be maximized and state-of-the-art Pt-on-carbon fuel cell catalysts usually range from 80 (2) to 100 m^2/g_{metal} (10), corresponding to particles in the range of 1.5 to 3 nm in diameter. The focus of the present work is to examine a commercially available carbon supported bimetallic Pt–Ru catalyst (11) in terms of particle size and the completeness of alloy formation using high resolution electron microscopy (HREM), electron, and X-ray diffraction, and microchemical analysis by energy dispersive X-ray spectroscopy (EDS).

The nanosize of these particles presents challenges to their microstructural characterization. Many of these challenges can be addressed by using transmission electron microscopy, especially for lattice structure characterization by high resolution electron microscopy, including the presence of defects as dislocations, twins, etc. The advantage of the application of TEM in catalyst characterization is described in several recently published review articles (12–14). HREM has been extensively used to determine faceting planes, i.e., its geometric shape, the presence of surface steps, surface roughness, as well as size and distribution of the Pt–Ru particles. Weak beam dark field imaging (WBDF) has not been used because of its well-known limitations if the particle size is less than 10 nm (14–17).

2. EXPERIMENTAL

2.1. Catalyst Preparation

The catalysts are commercially available (11) products made by a proprietary method. The method of preparation is similar to that described by Watanabe *et al.* (2), with the major difference being that both Ru and Pt are present in the impregnating solution as sulfite colloidal complexes. Briefly summarized, the preparation consists of the synthesis of Pt and Ru sulfite complexes in aqueous solution,

[1] Permanent address: University of Belgrade, Department of Physical Metallurgy, Karnegijeva 4, P.P.494, 11001 Belgrade, Yugoslavia.

0021-9517/95 $6.00

oxidative decomposition of the complex by the addition of hydrogen peroxide with simultaneous adsorption onto the carbon black (Vulcan XC-72R, Cabot Corp.) suspended in the solution. After water washing the catalyst was reduced in flowing hydrogen at 300°C. In this investigation, we examined two Pt–Ru catalysts having differing Pt : Ru ratios, denoted 1 (Pt : Ru = 1 : 1) and 2 (Pt : Ru = 3 : 1), but with the same metal loading (20 wt.%).

2.2. HREM

Specimens were prepared for transmission electron microscopy examination by ultrasonically suspending the catalyst powders in ethanol. A drop of suspension was then applied onto clean holey carbon grids and dried in air; in a second set of experiments, the catalyst powder was pressed onto copper grids. Samples were examined using the Topcon O2B and JEOL ARM high resolution electron microscopes at NCEM (18) as well as a JEOL 200CX analytical electron microscope. The particle shapes were determined by real space crystallography using high resolution electron microscopy images taken from the particles near or on the edge of the carbon black substrate. In order to get information about the overall distribution of Pt–Ru particles, dark-field imaging was also utilized.

To avoid contamination during energy dispersive X-ray spectroscopy (EDS) analysis, the microchemical analysis was performed at −160°C using a cold stage beryllium holder. This was found to be essential because of the time required for statistically significant spectral acquisition from samples with a particle size on the order of ≈2 nm (or particle clusters) using a 10-nm electron beam. The fluorescence effect can be neglected (19). Local structural information from single particles were obtained by numerical Fourier filtering of the digitized image intensity spectrum.

2.3. X-Ray Diffraction

X-ray diffraction data of samples 1 (Pt : Ru = 1 : 1) and 2 (Pt : Ru= 3 : 1) were acquired with a Siemens powder diffractometer (Model D500). The angular resolution in the 2θ-scans was 0.05° for the wide-angle 2θ-scans, and 0.02° for detailed scans about the (220) peak of the fcc (face-centered cubic) Pt–Ru alloy face. Spectral contributions of the copper $K\alpha_2$ line were subtracted prior to data analysis by a Rachinger algorithm correction (20), resulting in a symmetrical peak for the (220) face. The instrumental line broadening was measured under the same conditions on a homogenized Pt–Ru alloy sample with 30 at.% Ru (for a description of the bulk alloy preparation see Ref. 21), yielding a full width at half-maximum (FWHM) in the 2θ-scan, $B_{(20)}$, of 0.5°, thus marking the upper bound for the instrumental line broadening.

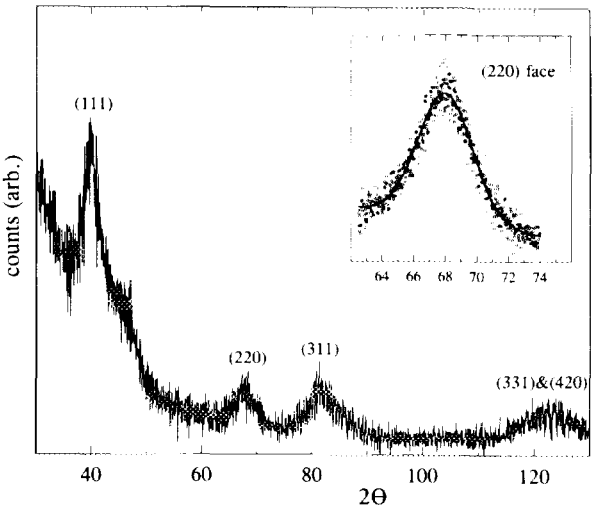

FIG. 1. X-ray diffraction pattern of a carbon-supported Pt–Ru catalyst (see Ref. 11) with an atomic ratio of Pt : Ru of 3 : 1. Diffraction peaks in the wide-angle 2θ-scan are indicated in the figure. The inset shows the detailed scan about the (220) fcc reflection of the Pt–Ru alloy clusters: (○) raw data; (—) least-squares fit to a Gaussian with linear background.

3. RESULTS AND DISCUSSION

3.1. X-Ray Diffraction Data Analysis

3.1.1. Wide-angle scans. Figures 1 and 2 show the X-ray diffraction patterns measured on the catalyst powders with Pt : Ru ratios of 3 : 1 and 1 : 1, respectively. Both samples exhibit only the characteristic diffraction peaks

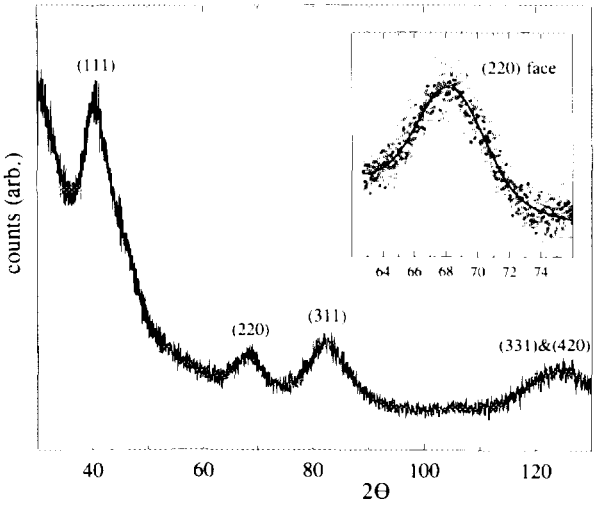

FIG. 2. X-ray diffraction pattern of a carbon-supported Pt–Ru catalyst (see Ref. 11) with an atomic ratio of Pt : Ru of 1 : 1. Diffraction peaks in the wide-angle 2θ-scan are indicated in the figure. The inset shows the detailed scan about the (220) fcc reflection of the Pt–Ru alloy clusters: (○) raw data; (—) least-squares fit to a Gaussian with linear background.

(marked in the figures) of the fcc Pt–Ru bulk alloys with a Ru concentration of less than ≈62 at.% (21). The merging of the closely spaced (331) and the (420) peaks ($\Delta_{(2\theta)} \approx 5°$) can be accounted for by particle size broadening, which increases with $1/\cos\theta$ (22), effecting a $B_{(2\theta)}$ of ≈6–8°, based on the width of the (220) peak and the particle sizes measured as described below. It is important to note that no diffraction peaks appear which would indicate the presence of an either pure Ru or Ru-rich hcp phase, so that it may be concluded that the catalysts are composed only of fcc Pt–Ru alloy particles. Furthermore, the absence of any superimposed sharp diffraction peaks indicates a unimodal particle distribution. This is in contrast to the report by Del Angel *et al.* (19) of both Pt–Ru clusters (<5 nm) and large (>50 nm) particles of pure Ru for a Pt–Ru catalyst supported on silica. This result reemphasizes the importance of matching the preparation chemistry with the surface chemistry of the support to achieve optimal bimetallic dispersion.

At the low 2θ range, in the vicinity of the (111) fcc diffraction peak of the alloys one can observe the strong background from the two-dimensional (10) reflection from individual carbon layers in the carbon black, following the analysis by Warren (23). The other two characteristic diffraction peaks for the carbon black in the recorded 2θ range are the (004) reflection at ≈55° and the (11) two-dimensional reflection at ≈78°. The latter is overlapping with the (311) diffraction of the fcc Pt–Ru alloy. Therefore, in order to assess both the particle size of the bimetallic clusters on the carbon support as well as to verify the high degree of alloy formation, i.e., composition homogeneity, we analyzed the (220) reflections in detail, the angular position of which is in a range where the diffraction spectrum of the carbon support only contributes in terms of a linear background.

3.1.2. (220) Diffraction peaks. Particle size broadening, after substraction of contributions from Cu$K\alpha_2$, should result in a Gaussian lineshape of the (220) reflection, convoluted with a linear background from the carbon support as outlined above. We therefore fitted the X-ray diffraction data to a Gaussian on a linear background, with the constraint that the slope be identical for both of the investigated samples, since it should be characteristic to the carbon itself. The pertinent results of a least-squares regression are summarized in Table 1 and are illustrated in the insets of Figs. 1 and 2. In general, the measured line broadening represents a convolution of the instrument broadening with the particle size broadening. As mentioned in Section 2, the instrumental broadening, $B_{(2\theta)\text{instr}}$ is less than 9 mrad (≤0.5°) and its convolution with the measured FWHM in Table 1, $B_{(2\theta)\text{measured}}$, changes the FWHM for the true particle size broadening only by ≈1%:

$$B_{(2\theta)\text{particle}} = \sqrt{B_{(2\theta)\text{measured}} - B_{(2\theta)\text{instr}}}. \quad [1]$$

This change is small compared to the ≈5% uncertainty in the measured $B_{(2\theta)}$ and will thus be neglected. Similarly, potential peak broadening induced by crystal strain is negligible compared to particle size broadening effects. Therefore, the average particle size, L, may be estimated from the parameters listed in Table 1 according to the Scherrer formula (22)

$$L = \frac{0.9\lambda_{K\alpha_1}}{B_{(2\theta)}\cos\theta_{\max}}, \quad [2]$$

where $\lambda_{K\alpha_1}$ is 1.54056 Å, and $B_{(2\theta)}$ is in radians. Hence, the average particle for the two catalysts with a Pt : Ru ratio of 3 : 1 and 1 : 1 is 2.3 and 1.9 nm, respectively, with an estimated error of ±6% based on the error bounds of the fitted parameters in Table 1 and assuming a unimodal particle size distribution (see Fig. 5).

The fcc lattice parameters for single-phase Pt–Ru bulk alloys (see Ref. 21) with Ru concentrations of less than 60 at.% are shown in Fig. 3, closely following a Vegard's Law relation, in excellent agreement with a previous study on cold-rolled alloy sheets (24). Lattice parameters can be evaluated from the angular position of the peak maxima ($\theta_{\max}$, Table 1)

$$a_{\text{fcc}} = \frac{\sqrt{2}\lambda_{K\alpha_1}}{\sin\theta_{\max}}, \quad (3)$$

yielding 0.3898 nm for sample 2 (Pt : Ru = 3 : 1), and 0.3884 nm for sample 1 (Pt : Ru = 1 : 1). The estimated error of ±0.5% for this measurement (indicated by the error bars in Fig. 3) is mainly due to the large penetration depth of the X-rays through the carbon matrix with its low absorption coefficient (see p. 71 in Ref. (22)), effecting diffraction throughout the entire thickness of the sample powder in the holder (≈1 mm). Even though this large error does not allow for the assessment of the sample composition from measured lattice parameter values, the decrease in

TABLE 1

Peak Position and FWHM Derived from a Five-Parameter Least-Squares Fit of the (220) Diffraction Data to a Gaussian Lineshape with Linear Background

	Pt : Ru = 3 : 1 (see Fig. 1)	Pt : Ru = 1 : 1 (see Fig. 2)
$2\theta_{\max}$ (°)	67.96 ± 0.05	68.24 ± 0.08
$B_{(2\theta)}$ (mrad)	71.0 ± 2.6	86.4 ± 4.8

Note. The curves resulting from these data are plotted in the insets of Figs. 1 and 2. The overall regression coefficient r^2, is 0.949, and the given errors represent the 99% confidence limits. The slope of the background was constrained to be identical for both samples.

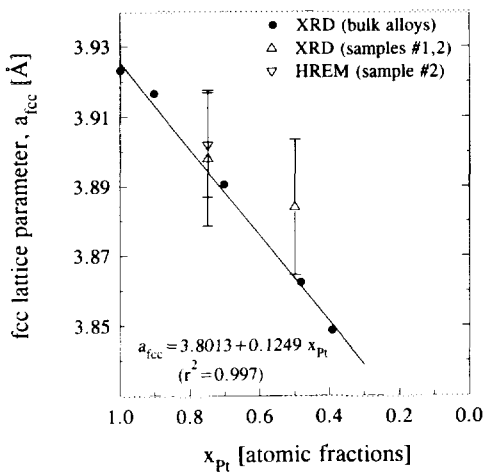

FIG. 3. Fcc lattice parameters for Pt–Ru bulk alloys versus the atomic fraction of Pt (see Ref. 21). The linear regression fit to Vegard's Law is shown in the figure as well as lattice parameters of carbon supported Pt–Ru particles measured by XRD and HREM.

the lattice parameter with increasing Ru concentration does lend further support to the idea that the supported bimetallic catalysts are indeed a solid solution of Pt and Ru, rather than a physical mixture of particles of the two metals.

3.2. High Resolution Electron Microscopy

Typical conventional TEM bright field and dark field images of the Pt–Ru catalysts are shown in Figs, 4a and b. The dark field image is taken using the (002) diffraction ring (see inset to Fig. 4). The dark field images indicate qualitatively that the particle size is relatively small, e.g., <10 nm. Both images show that the distribution of the metal particles on the carbon support is reasonably uniform, an especially important characteristic for an electrocatalyst (25).

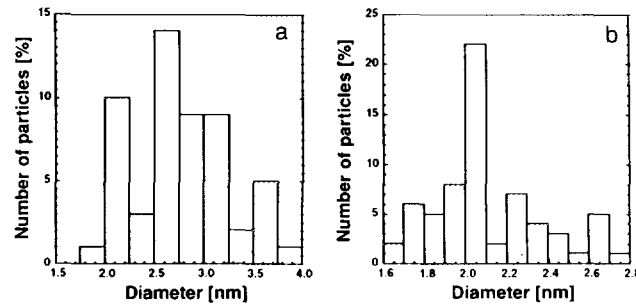

FIG. 5. Histograms of the Pt–Ru particles size distribution in the catalysts with Pt : Ru ratios 3 : 1 (a) and 1 : 1 (b).

Both the 1 : 1 and 3 : 1 catalyst have similar particle size and morphology. Histograms of the particle size distributions in the two catalysts are shown in Fig. 5. These histograms include analyses of several different regions in the same catalyst, including some regions where the metal particle distribution was less uniform than in Fig. 4, e.g., much more concentrated. Nonetheless, the particle size distribution is remarkably uniform, with the average particle size being ca. 2 nm for both catalysts in good agreement with the XRD measurements (see Section 3.1).

Two-dimensional projections, such as those in Fig. 6, give the impression of spherical or elliptical shapes, as opposed to faceted shapes such as cubooctahedral–octahedral. However, apparent rounding of particles can be caused by two effects: due to the inclination of the particles from the low index zone axis, faceted corners appear to be slightly curved; even when particles are aligned along a low index zone axis they can appear to be spherical because of interference from the carbon substrate and confusing contrast (e.g., as in (26) that obscures sharp edges and corners. The latter effect can be avoided by analyzing particles close to the edge of the carbon support, such as those shown in Fig. 7. Detailed analyses of parti-

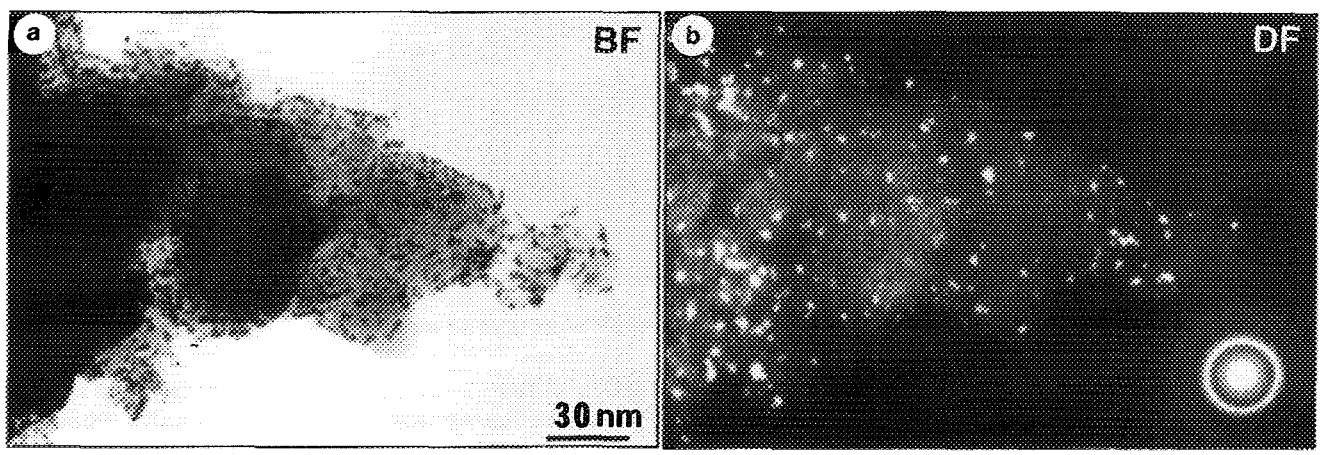

FIG. 4. A typical conventional TEM bright field (a) and dark field (b) image of investigated Pt–Ru catalyst; the dark field is taken using 111 ring intensity (see inset).

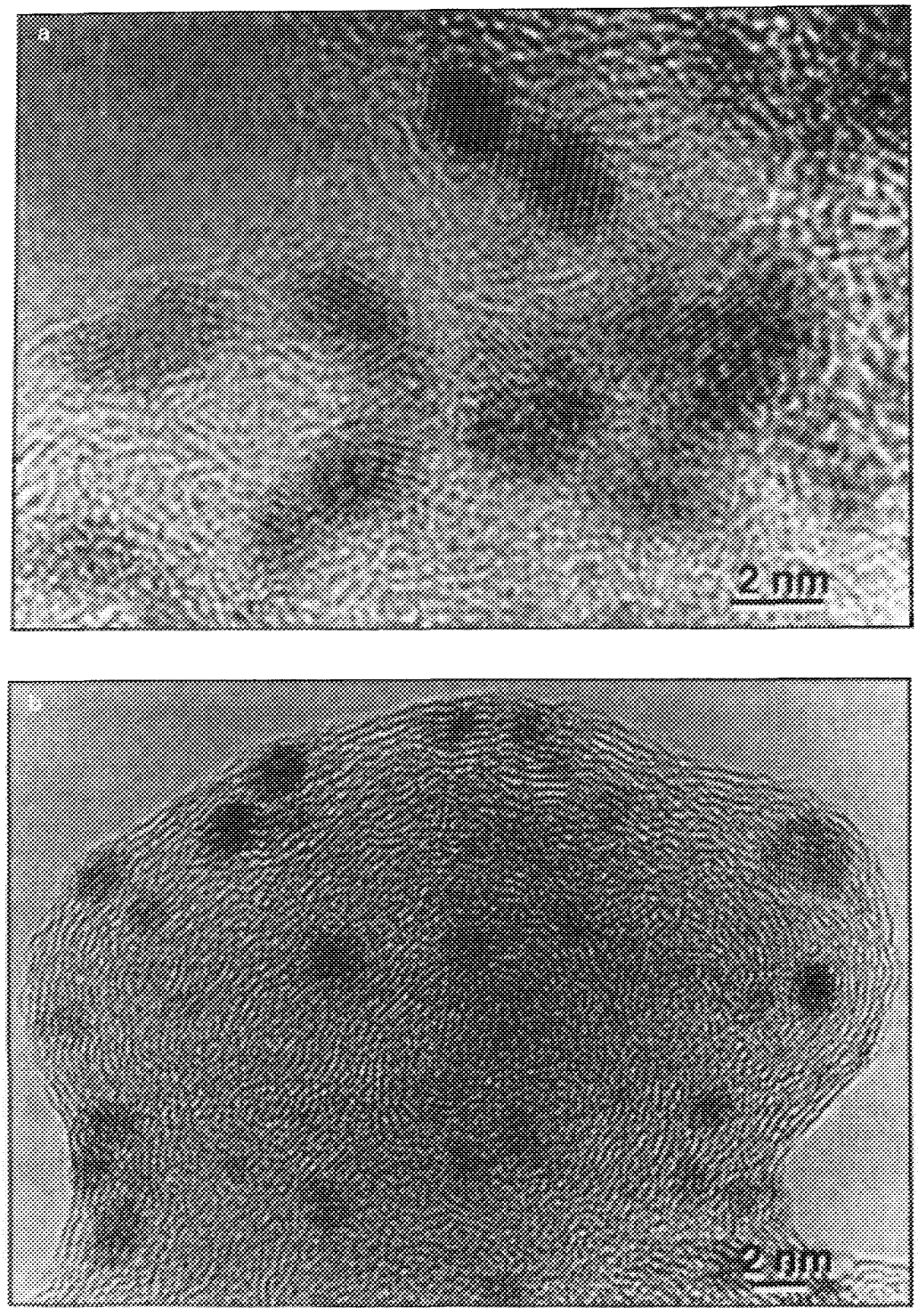

FIG. 6. (a) Low magnification HREM micrograph of Pt–Ru catalysts supported on black carbon: (a) Pt : Ru = 3 : 1; (b) Pt : Ru = 1 : 1.

cles on or close to the edges of the carbon support show they are faceted on (111) and (200) planes, characteristic of fcc asymmetric or symmetric cubooctahedral nanocrystals. However, the majority of the particles in the catalysts are not conveniently located on edges of the carbon substrate, so that analysis of only these particles may not be representative of the catalyst as a whole. The contrast problem with particles on the thick regions of the carbon were reduced by using Fourier filtering, which can remove much of the contribution from the incoherent

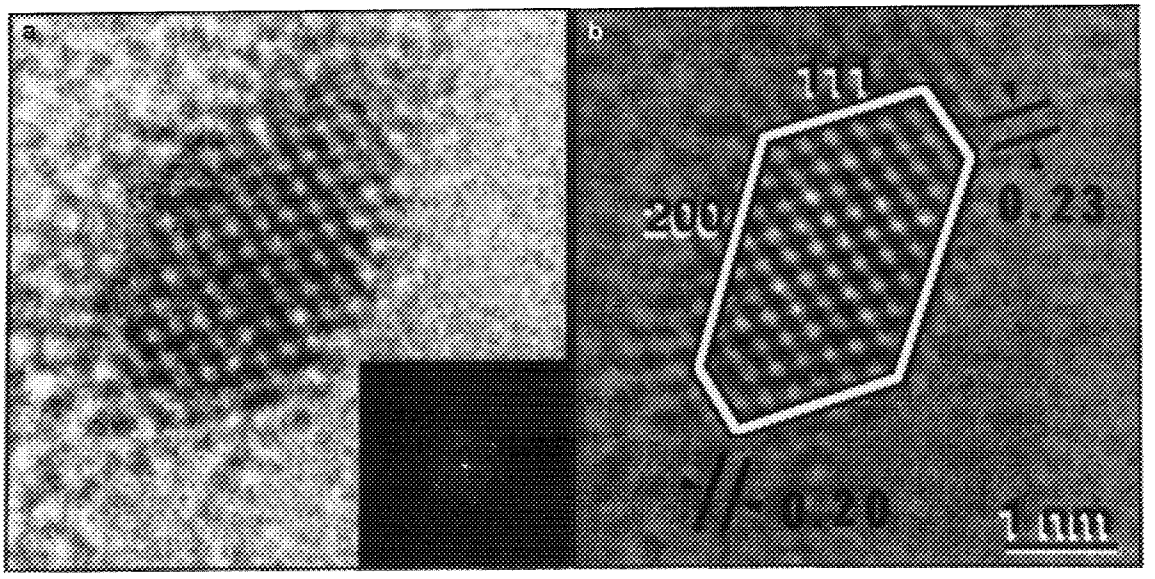

FIG. 7. HREM micrograph of a carbon-supported Pt–Ru particle (Pt : Ru = 3 : 1) on the edge of the carbon support: (a) unfiltered image of asymmetric cubooctahedral particle (inset: 110 microdiffraction pattern); (b) Fourier filtered image.

scattering of electrons from the amorphous carbon. As shown in Fig. 8, Fourier filtered images from particles in the interior of catalyst still reveal faceted shapes, typically cubooctohedral.

The nominally 0.2 and 0.23 nm spacings of the (002) and (111) planes, respectively, of the fcc lattice of a typical faceted particle is indicated by the arrows in Fig. 7b. More accurate measurements of the lattice spacing were made using a Cu grid as an internal calibration (Fig. 9a). Lattice spacings measured on different particles in the same catalyst varied by about ±0.4%, essentially the same variation as the precision of the lattice parameter measurement in Fig. 9 (±1 pixel out of 256). A typical result is shown in Fig. 9b for a single particle in the nominally 3 : 1 catalyst. The lattice constant from the spacing of the (111) planes is 0.3902 ± 0.0015 nm in reasonable agreement for the value for the 3 : 1 bulk alloy (Fig. 3, 0.3895 nm) and again in close agreement with the XRD measurements. However, the lattice constant measurement from interplanar spacing does not have sufficient accuracy to determine compositional variations between particles beyond extremes, e.g., pure Ru and Ru-rich phases, since ±1% covers the whole range of lattice parameters between pure Pt and 1 : 1 Pt : Ru (Fig. 3).

The electron diffraction patterns, including the single-particle microdiffraction pattern shown in Fig. 10, were characteristic of only Pt-rich fcc phases. The beam size was 10 nm, well above the average particle size, so that observed additional weak diffraction spots (other than 112 spots) probably derive from the partial sampling of neighboring particles. No pure Ru or Ru-rich hcp particles were observed. The EDS analyses, summarized in Table 2, show that regardless sof the beam size and/or particle size(s) under the beam, the Pt : Ru ratio was always the same and in reasonable agreement with the nominal composition of the catalyst, i.e., 1 : 1 and 3 : 1. All of the

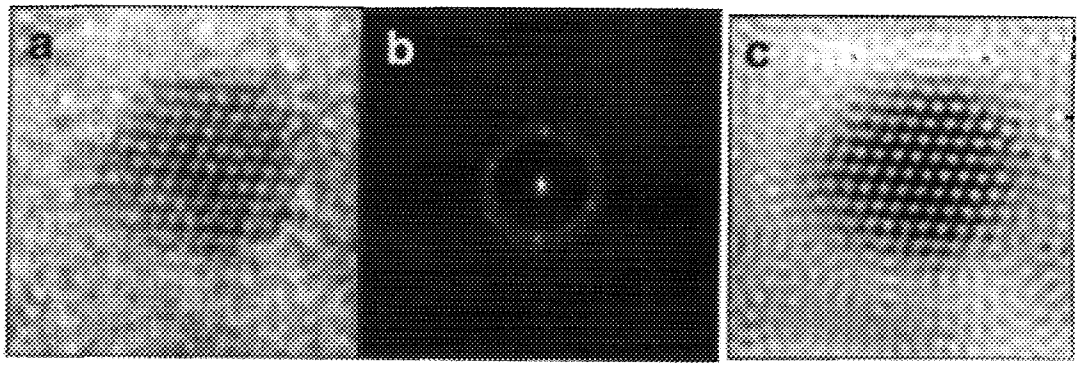

FIG. 8. HREM micrograph of carbon a supported Pt–Ru particle (Pt : Ru = 3 : 1) in the interior region of the catalyst. (a) unfiltered image of symmetric cubooctahedral particle; (b) microdiffraction pattern); (c) Fourier filtered image.

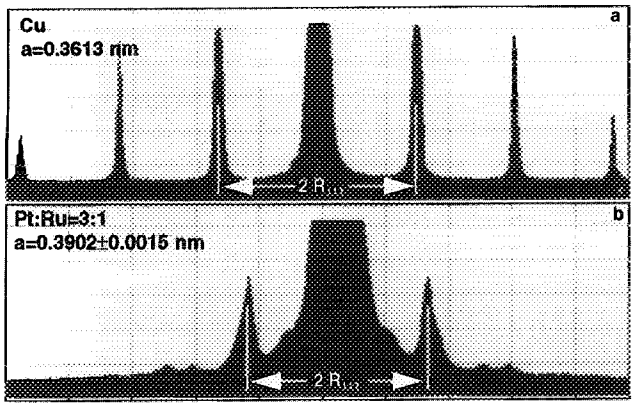

FIG. 9. Digitized selected area electron diffraction pattern from the catalyst containing Pt and Ru in the ratio 3 : 1 obtained at 800 kV in the ARM electron microscope. (a) Calibration of the camera constant using the Cu grid; (b) microdiffraction from the catalyst sample.

microscopic characterizations indicate that essentially all of the metal particles are bimetallic nanocrystals having nearly identical compositions and approximately the same size.

Occasionally, particles having {113} facets and twinned particles were also observed. Although these features were atypical, their existence in these catalysts is noteworthy, since we have *never* seen either twins or {113} facets in pure Pt catalysts on the same support pretreated in the same way. An example of the simultaneous occurrence of both in the same particle is shown in Fig. 11. This particle has the same (111) twinning plane as in other fcc metals. The almost perfect {113} facet does not appear to be accompanied by any relaxation in the interatomic spacing near the surface, as might occur with a surface enriched in one element relative to the bulk, but as we stated above, the change in interplanar spacing in this alloy is too small to be observed by lattice imaging. The fact that these unusual features are correlated to the existence of Ru atoms in the particles suggests that their occurrence may be related also to the effect of Ru on the bulk lattice, e.g., residual stress due to the expected composition gradient between the surface and the bulk (21).

The investigated Pt–Ru particles supported on carbon black were observed to be relatively stable under irradiation, and a shape change under illumination has not been observed, as reported for ultrafine gold particles, supported on amorphous Si and SiO_2 (27), MgO (28), or TiO_2 substrate (29), and in several other pure metals supported on carbon black (30, 31), including Pt (15). Marks and coworkers (32) suggested that the reason for this behavior could be a relatively small activation barrier (a few electron volts) for transformations between different shapes compared to the energy deposited by the electron beam (200 to 1000 eV). This suggests that stability of Pt–Ru particles can be related to their bimetallic nature or the presence of Ru in Pt-based solid solution. Since our observation indicates higher stability of Pt–Ru particles than pure Pt, it suggests that Ru possibly increases the activation barrier for shape transformation.

Finally, we consider the very important question, from

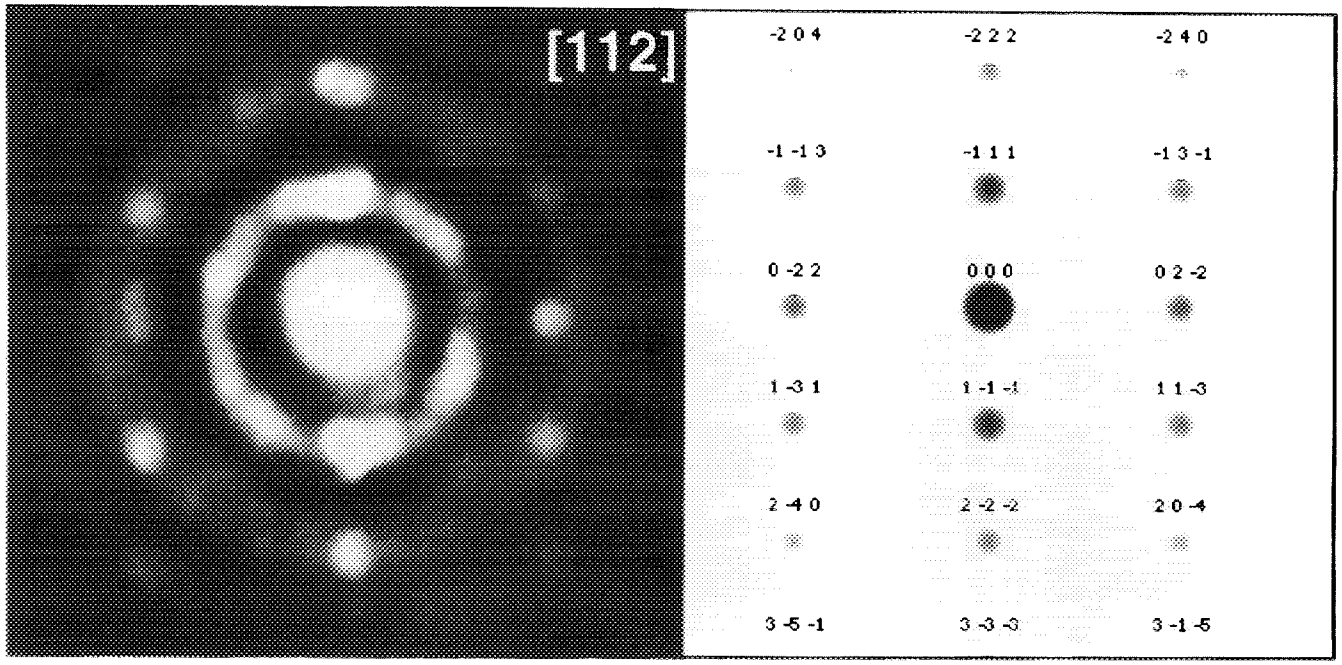

FIG. 10. Microdiffraction of small Pt–Ru (3 : 1 ratio) particle in [112] zone axis obtained at 200 kV in the JEM-200CX electron microscope (left); calculated fcc diffraction pattern for the [112] zone axis (right).

TABLE 2

X-Ray Microanalysis of Investigated Pt–Ru Particles (at.%)

Analysis	Ru	Pt	Beam (nm)	Remarks
		Catalyst 2 (nominal ratio pt : Ru = 3 : 1)		
1	25.1	74.9	10	Particle 3 nm
2	24.8	75.2	10	Bulk
3	24.7	75.3	10	Bulk
4	24.7	75.3	30	Cluster 30 nm
Average	24.8	75.2		
		Catalyst 1 (nominal ratio Pt : Ru = 1 : 1)		
1	49.2	50.8	20	Cluster 50 nm
2	49.0	51.0	20	Cluster 60 nm
3	52.1	47.9	20	Cluster 10 nm
4	52.1	47.9	20	Bulk
5	49.2	50.8	20	Cluster 30 nm
6	52.9	47.1	20	Cluster 20 nm
Average	50.75	49.25		

a catalytic standpoint, of the surface composition of the particles. In bulk Pt–Ru alloys of 1 : 1 and 3 : 1 composition, the clean annealed surface is considerably enriched in Pt (21) due to the lower surface tension of Pt and a nearly zero heat of mixing (33). This enrichment results in a surface composition (21) which is a nearly constant 87% Pt (±5%) for bulk compositions from 20–60% Pt and thus has a (serendipitous) beneficial effect on the catalytic activity of the alloy, since the optimum surface composition for methanol electrooxidation (9) is ca. 90% Pt. One might expect to be able to observe surface enrichment by HREM by the measurement of the surface relaxation in individual particles, especially particles on the very edge of the carbon substrate. Surface relaxation measurements are not straightforward, as pointed out by Gibson (34) in his discussion of the measurements of the surface relaxation on gold particles by Marks and Heine (35). There is also a contribution of the sample tilt and uncertainties in the exact direction of the surface normal that can be misinterpreted as part of the surface relaxation, as shown by Malm and O'Keefe (36). According to their calculations (36), the errors in the measurement of interplanar relaxation in high resolution images are on the order of a few percent, and can be as high as 10%. Since the surface relaxation even for a pure Pt surface layer on top of an alloy bulk lattice would only be ca. 2%, we concluded it was not possible to make any determination by HREM about surface composition in these catalysts. However, the catalytic activity of the two catalysts for methanol electrooxidation was essentially the same, which is the expected result for alloys of these bulk compositions only when the surfaces have the equilibrated (enriched) composition; if the surfaces of these two catalysts had the bulk compositions, the activities would have differed by about an order of magnitude (9).

5. CONCLUSIONS

Based on the analysis of the Pt–Ru electrocatalysts supported on carbon black using the combination of X-ray diffraction and high resolution and analytical electron microscopy, we made the following conclusions:

(i) The presence of Ru in the catalyst appeared to have relatively little effect on the resulting particle size, with the average particle size being ca. 2–3 nm for both the 3 : 1 and 1 : 1 (Pt : Ru) catalysts, which is also about the same particle size as for pure Pt particles on the same support. The particle size distribution (by HREM) for 90% of the particles was ±0.5 nm and ±0.2 nm for the catalysts with a Pt : Ru ratio of 3 : 1 and 1 : 1, respectively.

(ii) The particles are essentially uniform in composition, having the same composition as the nominal composition of the bulk catalyst. Thus, the particles are all fcc alloy nanocrystals of Ru in a Pt solid solution. We were unable to determine if there is any surface segregation (enrichment in Pt) in the individual nanocrystals.

(iii) The majority of the particles are truncated by the (111) and (200) crystallographic planes and are cuboctahedral in shape, as observed in pure Pt and in many other fcc metal nanocrystals. However, occasionally {113} type facets that are not typical of fcc nanocrystals were observed, and occasionally twinned particles were also observed, which is not generally the case for pure Pt particles on the same carbon support.

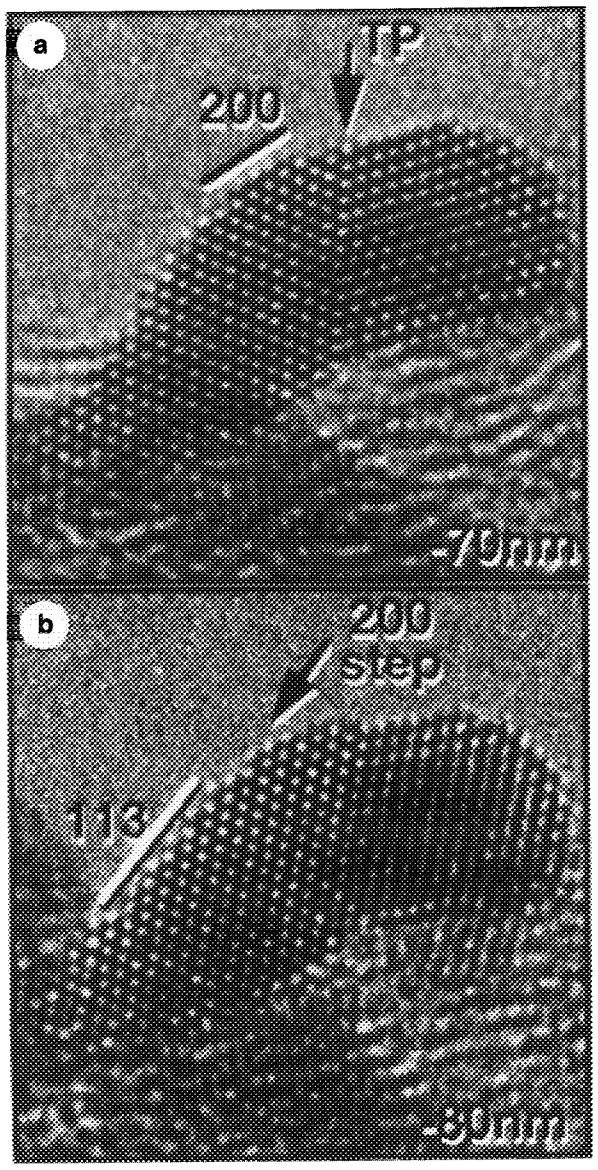

FIG. 11. High resolsution electron micrograph of a twinned particle found in Pt–Ru (3 : 1) catalyst: (a) −70 nm defocus setting; (b) −80 nm defocus setting. {113}, {200} facets and the twinning plane are indicated in the figure.

ACKNOWLEDGMENTS

This work was supported by the Assistant Secretary for Energy Efficiency and Renewable Energy, Office of Transportation Technologies, Electric & Hybrid Propulsion Division of the U. S. Department of Energy under Contract DE-AC03-76SF00098. Funding for NCEM is provided by the Office of Basic Energy Sciences, Division of Materials Sciences, U. S. DOE under Contract DE-AC03-76SF00098. V.R. acknowledges the invaluable assistance of John Turner.

REFERENCES

1. Cameron, D. S., Hards, G. A., and Thompsett, D., *in* "Proceedings of the Workshop on Direct Methanol–Air Fuel Cells" (A. R. Landgrebe, R. K. Sen, and D. J. Wheeler, Eds.), Vol. 92–14, p. 10. The Electrochemical Society, Pennington, NJ, 1992.
2. Watanabe, M., Uchida, M., and Motoo, S., *J. Electroanal. Chem.* **229,** 395 (1987).
3. Wasmus, S., and Vielstich, W., *J. Appl. Electrochem.* **23,** 120 (1993).
4. Miura, H., and Gonzalez, R. D., *J. Catal.* **74,** 216 (1982).
5. Garin, F., and Maire, G., *J. Mol. Catal.* **52,** 147 (1989).
6. Villamil, P., Lopez, A., and Gomez, R., *React. Kinet. Catal. Lett.* **32,** 475 (1986).
7. Miura, H., Suzuki, T., Ushikubo, Y., Sugiyama, K., Matsuda, T., and Gonzalez, R. D., *J. Catal.* **85,** 331 (1984).
8. Alerasool, S., and Gonzalez, R. D., *J. Catal.* **124,** 204 (1990).
9. Gasteiger, H. A., Marković, N., Ross, P. N., Jr., and Cairns, E. J., *J. Phys. Chem.* **97,** 12020 (1993).
10. Wilson, M. S., Garzon, F. H., Sickafus, K. E., and Gottesfeld, S., *J. Electrochem. Soc.* **140,** 2872 (1993).
11. The two investigated catalyst samples were provided by E-TEK Inc. (Natick, MA) and had a metal loading of 20 wt% on Vulcan XC-72 with atomic ratios of Pt to Ru of 1 : 1, and 3 : 1, respectively. Prior to our analysis, the catalyst was reduced in flowing H_2 at 250°C.
12. Datye, A. K., and Smith, D. J., *Catal. Rev.-Sci. Eng.* **34,** 129 (1992).
13. Yacaman, M. J., and Avalos-Borja, M., *Catal. Rev.-Sci. Eng.* **34,** 55 (1992).
14. Popa, H., *Catal. Rev.-Sci. Eng.* **35,** 359 (1993).
15. Sattler, M. L., and Ross, P. N., *Ultramicroscopy* **20,** 21 (1986).
16. Smith, D. J., and Marks, L. D., *Ultramicroscopy* **16,** 101 (1985).
17. Yacaman, M. J., and Dominguez, J. M., *J. Catal.* **64,** 23 (1980).
18. National Center for Electron Microscopy Users Guide, Lawrence Berkeley Laboratory, Berkeley, CA 94720, PUB-475.
19. Del Angel, G., Alerasool, S., Domingues, J. M., Gonzalez, R. D., and Gomez, R., *Surf. Sci.* **224,** 407 (1989).
20. The Rachinger correction was carried out with the instrument controlling software (Diffrac-AT v.3.1).
21. Gasteiger, H. A., Ross, P. N., Jr., and Carins, E. J., *Surf. Sci.* **293,** 67 (1993).
22. Warren, B. E., "X-ray Diffraction." Addison–Wesley, Reading, MA, 1969.
23. Warren, B. E., *in* "Proceedings First and Second Conferences on Carbon Buffalo, NY, 1956" p. 49. Waverly Press, Baltimore, 1956.
24. Binder, H., Köhling, A., and Sandstede, G., *in* "From Electrocatalysis to Fuel Cells" (G. Sandstede, Ed.), p. 43. Univ. of Washington Press, Seattle, 1972.
25. Kunz, H. R., and Gruver, G., *J. Electrochem. Soc.* **122,** 1279 (1975).
26. Chojanacki, T., Krause, K., and Schmidt, L. D., *J. Catal.* **128,** 161 (1991).
27. Iijima, S., and Ichihashi, T., *Phys. Rev. Lett.* **56,** 616 (1986).
28. Marks, L. D., and Ajayan, P. M., *Phys. Rev. Lett.* **63,** 279 (1989).
29. Fuchs, G., Neiman, D., and Poppa, H., *Langmuir* **7,** 2853 (1991).
30. Yao, M.-H., Smsith, D. J., and Datye, A.K., *Ultramicroscopy* **52,** 282 (1993).
31. Dahmen, U., *MRS Bulletin* **24,** 341 (1994).
32. Dundurs, J., Marks, L. D., and Ajayan, P. M., *Philos. Mag. A* **57,** 605 (1988).
33. Miedema, A. R., *Philips Tech. Rev.* **36,** 217 (1976).
34. Gibson, J. M., *Phys. Rev. Lett.* **52,** 656 (1984).
35. Marks, L. D., and Heine, V., *Phys. Rev. Lett.* **52,** 656 (1984).
36. Malm, J.-O., and O'Keefe, M. A., *Proc. EMSA* (1993), p. 974.